Supporting Information

An Insight into The Significant Contribution of Intrinsic Carbon Defects for High-Performance Capacitive Desalination of Brackish Water

Silu Huo,[ab] *Xue Song,*[ab] *Yubo Zhao,*[ab] *Wei Ni,*[c] *Hao Wang,* *[ab] *Kexun Li* *[ab]

a: The College of Environmental Science and Engineering, Nankai University, Tianjin 300071, China
b: MOE Key Laboratory of Pollution Processes and Environmental Criteria, Tianjin Key Laboratory of Environmental Remediation and Pollution Control, Tianjin Key Laboratory of Environmental Technology for Complex Trans-Media Pollution, Nankai University, Tianjin 300071, China
c: Beijing Aerospace Propulsion Institute, Beijing, 100076 China

*Corresponding Author.

Email: likx@nankai.edu.cn; Hao_WangNKU@163.com

S1. Materials and methods

S1.1. Materials

Sodium chloride, Zinc chloride and sucrose were purchased from Aladdin Chemical Reagent Co. Ltd. All the aqueous solution used in experiments were deionized (DI) water and all chemical reagents were analytical grade.

S1.2 Synthesis of carbons with different degrees of intrinsic defects

For DT-PC sample, typically, 1.0 g sucrose was dispersed in 20 mL deionized water, followed by addition of 10 g NaCl and 1.0 g $ZnCl_2$ while stirring. The mixture was frozen to the solid state by liquid nitrogen several minutes and the ice cube was freeze-dried for 2 d to remove water. Freeze-drying condition is -50 °C and 20 Pa. Afterwards, the freeze-dried sample was heated in a tube furnace at 700 °C for 2 h at argon atmosphere. After cooling to room temperature, the obtained black carbonization product was washed thoroughly with 0.5 M HCl and DI water to remove the inorganic impurities then dried at 80 °C for 24 h. For comparison, the ST-PC sample was prepared by the same procedure of DT-PC, only without adding $ZnCl_2$. Similarly, the NT-C was prepared using the same synthesis of DT-PC, but without addition of NaCl and $ZnCl_2$.

S1.4. Materials Characterization

The nanostructure of carbons was characterized by field emission scanning electron microscopy (FE-SEM, Ultra Plus, Carl Zeiss, Germany) at an accelerating voltage of 5.0 kV and a transmission electron microscopy (TEM, JEM-2010 Japan). Elemental mappings were performed on the energy-dispersive X-ray (EDX) spectroscope attached to Tecnai G2 F30. Raman spectra was recorded with a Raman spectrometer (Renishaw) with an argon ion laser (λ=514 nm). The Brunauer-Emmett-Teller surface area of the obtained samples was tested by nitrogen adsorption-desorption in a Micromeritics ASAP 2020 nitrogen adsorption apparatus. And the pretreatment was conducted at 300

°C for 3 h to exhaust the adsorbed gas. The X-ray diffraction (XRD) test was performed on a diffractometer (D/Max-2400, Rigaku) advance instrument using Cu Kα radiation (k =1.5418 Å) at 40 kV, 100 mA. The X-ray photoelectron spectroscopy (XPS) measurement was conducted on an Escalab 210 system (Germany) using a monochromatic Al Kα radiation source (ThermoVG Scientific). Electron paramagnetic resonance (EPR) measurements were performed on a Bruker EMXplus EPR spectrometer at room temperature. Mercury intrusion porosimetry was obtained by AutoPore IV 9510. The content of elements was measured by an elemental analyzer (Flash EA 1112) and inductively coupled plasma-optical emission spectroscopy (ICP-OES, Varian 710).

S1.5 Electrochemical measurements

S1.5.1 Electrochemical characterization

Electrodes were prepared by mixing 80 wt. % of active material with 10 wt. % of polytetrafluoroethylene (PTFE) binder (Aldrich, 60 wt. % suspension in water) and 10.0 wt. % carbon black in ethanol and then coated onto the graphite paper current collectors. The prefabricated electrodes dried at 80 °C for 12 h in a vacuum oven and were pressed under a pressure of 20 MPa for 3.0 min. The capacitive performance of electrode in three-electrode system was investigated in 1.0 M NaCl aqueous solution by a CHI760D electrochemical workstation (Chenhua Instruments Inc., Shanghai, China) with platinum wire and Hg/HgO electrode as counter and reference electrodes, respectively. Cyclic voltammetry (CV) test, galvanostatic charge-discharge (GCD) method and electrochemical impedance spectroscopy (EIS) analysis were conducted in the electrochemical studies. The specific capacitance derived from GCD was calculated by the equation: $Cg = \frac{I}{mdV/dt}$, where I is the constant current and m is the mass of

active materials, as well as dV/dt is the slope obtained from fitting the discharge curve from the end of the voltage drop to the end of the discharge process. The specific capacitance derived from CV was calculated by the equation: $Cg = \frac{\int_{V1}^{V2} IdV}{2v\Delta Vm}$, where I is the response current (A), V_1 and V_2 represent the starting and ending potential, respectively, ΔV is the applied potential window (V), v is the potential scan rate (V/s), and m is the mass of active electrode material (g).

S1.5.2 CDI characterization

For CDI characterization, we used the graphite paper as current collector, while the electrode materials were coated by a conventional blade coating method. For each electrode, the active material quality is 25 mg. The thickness of the electrode is approximately 0.4 mm and the single electrode area is 25 mm × 25 mm. The distance between the electrodes is 2 mm. The volume of NaCl solution used is 60 ml. The peristaltic pumps drive the circulating flow of the NaCl solution at a flow rate of 10 mL min^{-1}. The conductivity meter is used to record the conductivity value of the NaCl solution flowing form the CDI device. The salt adsorption capacity (SAC, mg g^{-1}) was calculated according to the equation: $SAC = \frac{(c0 - c)Vs}{w}$, where C0 and C represent the initial and the final salt concentration (mg L^{-1}), and Vs is the volume of NaCl solution (L), as well as w is the total mass of active materials. The charge efficiency could obtain from the equation: $\varphi = \frac{SAC * F}{C}$, in which the SAC represents salt adsorption capacity (mg g^{-1}), F is the Faraday constant 96485 (C mol^{-1}) and C is calculated by integrating the charge current (C g^{-1}). Kim-Yoon plot was to evaluate the relationship between the salt adsorption capacity and the mean salt adsorption rate at the corresponding moment.

The salt adsorption capacity (SACt, mg g^{-1}) and the salt adsorption rate (SAR, mg g^{-1} min^{-1}) at t minute were calculated by the following equations: $SACt = \frac{(C0 - Ct)Vs}{w}$ and $SAR = \frac{SACt}{t}$. The Ct is the concentration of NaCl solution at t minute and t (min) is the desalination process time.

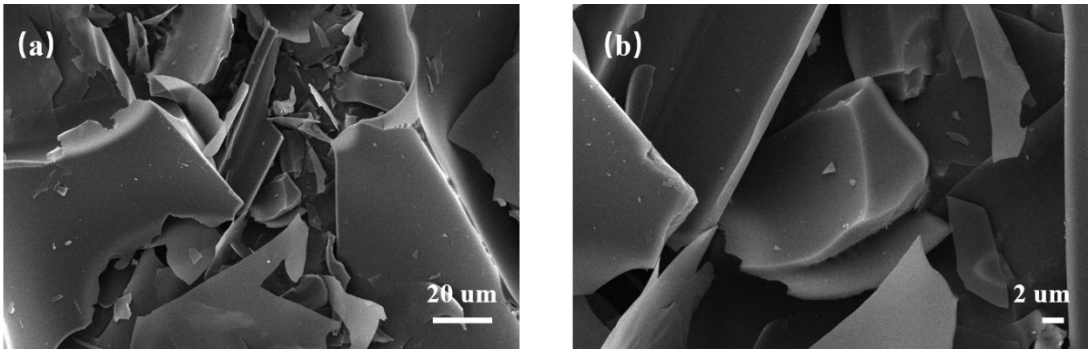

Figure S1. (a-c) SEM images of NT-C.

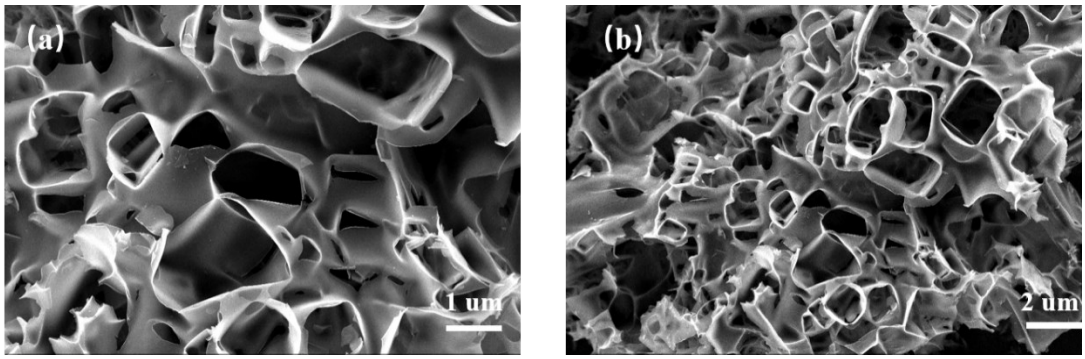

Figure S2. (a-b) SEM images of ST-PC.

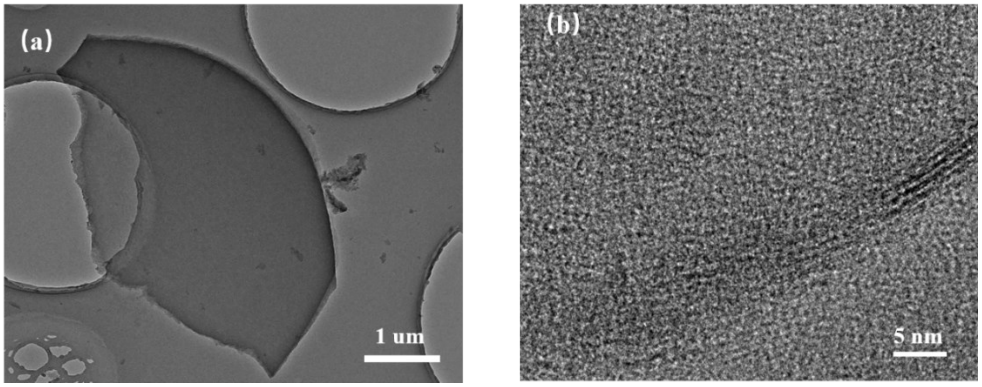

Figure S3. (a-b) TEM images of NT-C sample.

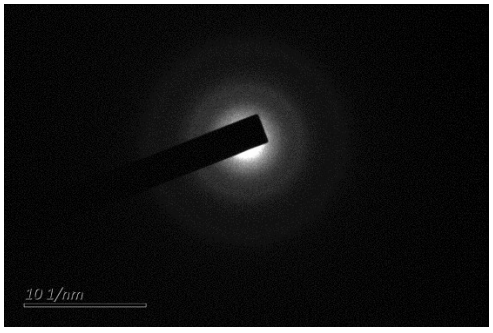

Figure S4. Selected area electron diffraction of DT-PC.

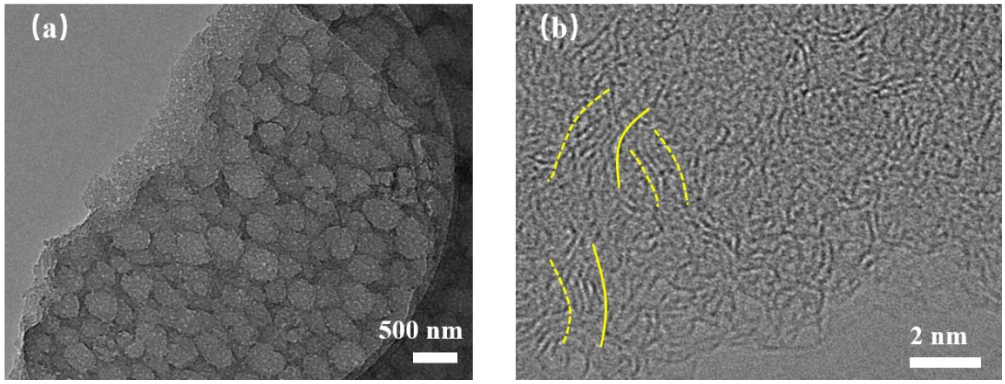

Figure S5. (a-b) TEM images of ST-PC.

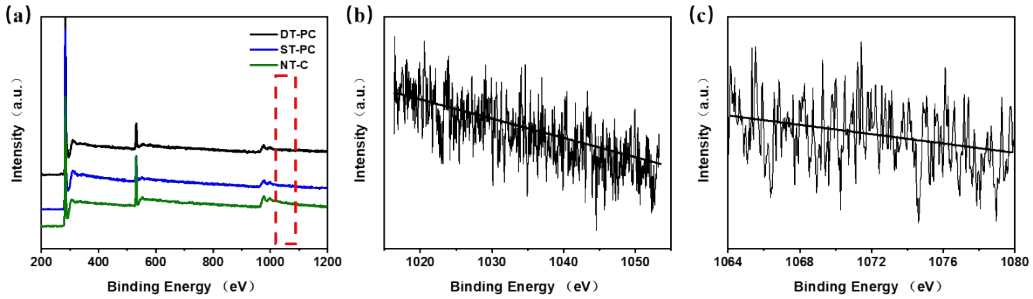

Figure S6. (a) Full-scale XPS spectra of DT-PC, ST-PC and NT-C. (b) Zn 2p. (c) Na 1s of DT-PC.

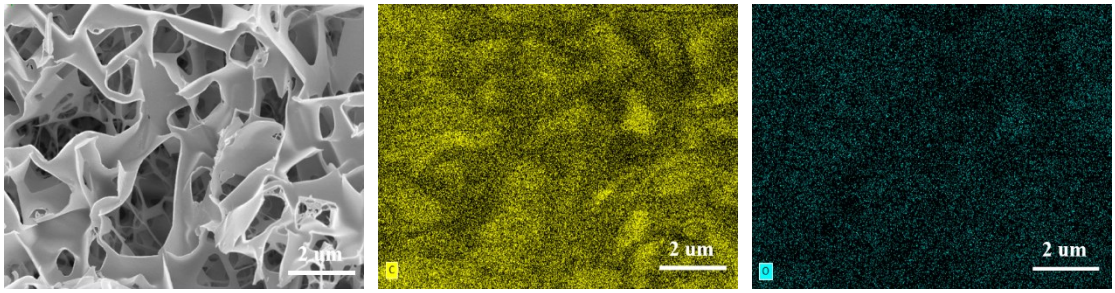

Figure S7. Energy-dispersive X-ray spectroscopy of DT-PC sample.

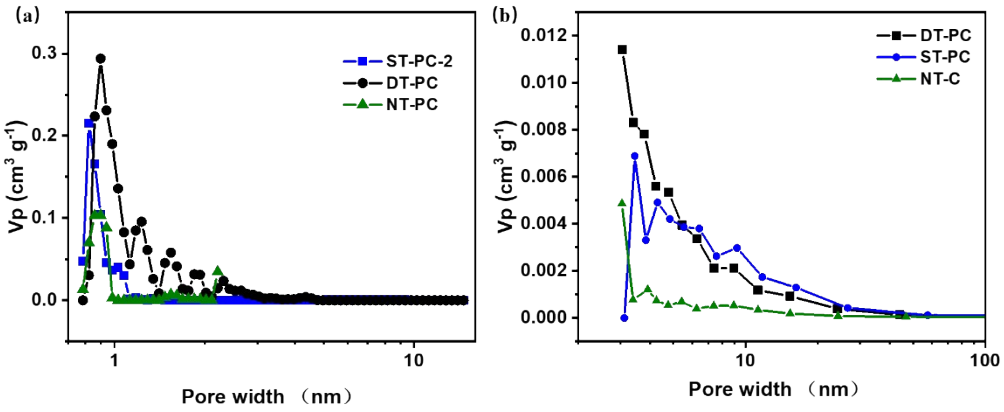

Figure S8. pore size distribution profiles.

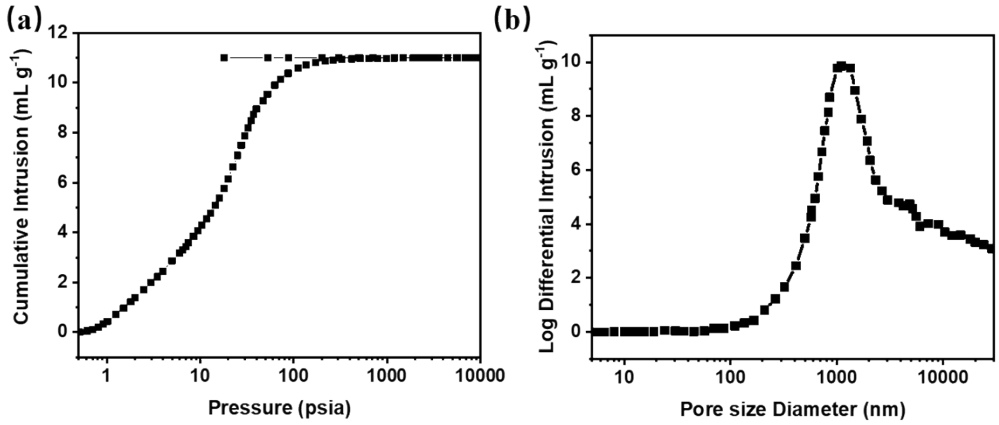

Figure S9. Cumulative intrusion and pore size distribution via mercury porosimetry of DT-PC.

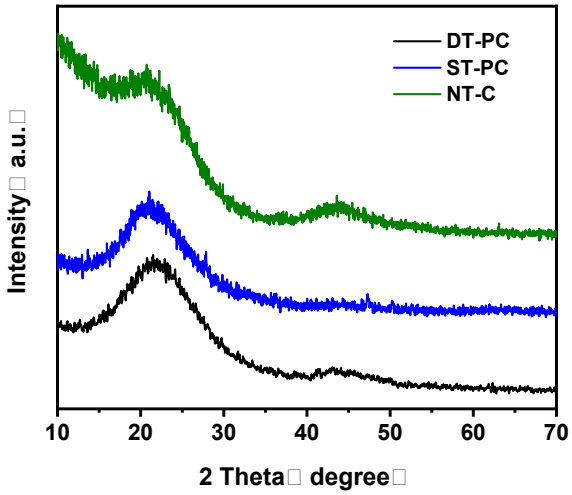

Figure S10. XRD patterns of all carbon samples.

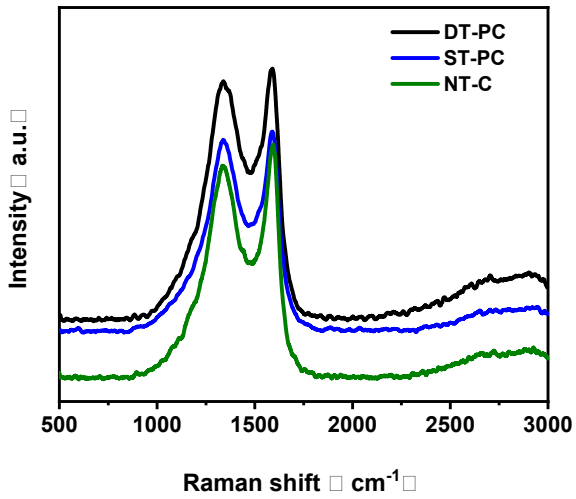

Figure S11. Raman spectrums of all carbons.

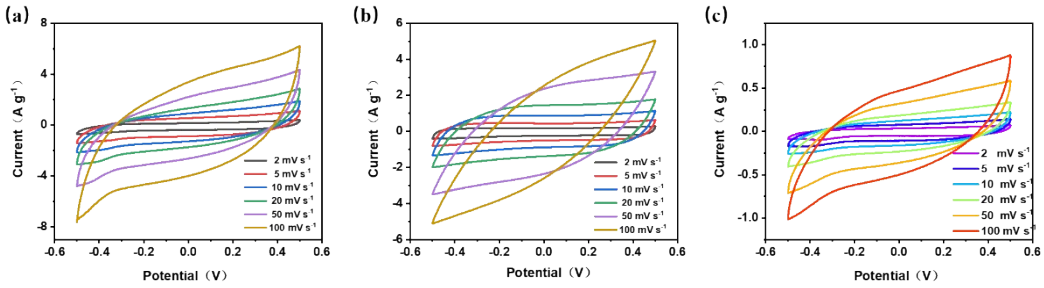

Figure S12. CVs of (a) ST-PC. (b) AC. (c) NT-C.

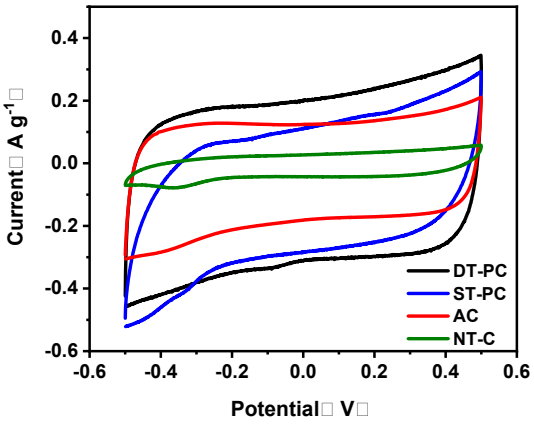

Figure S13. CVs at 1 mV $s^{-1}$of DT-PC, ST-PC, AC and NT-C.

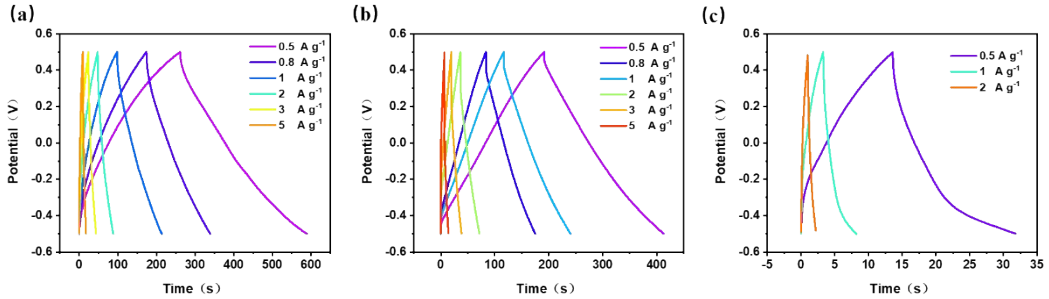

Figure S14. GCD curves at current densities of 0.5 to 5 A g^{-1}. (a) ST-PC. (b) AC. (c) NT-C.

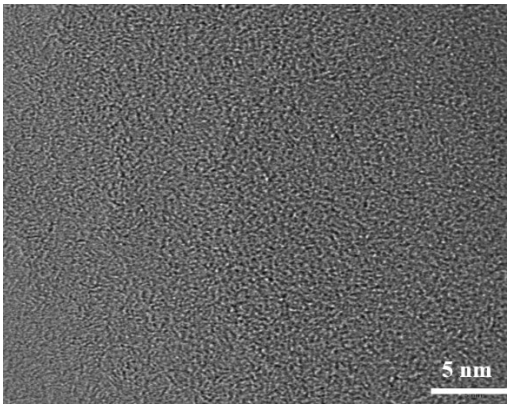

Figure S15. HRTEM image of AC.

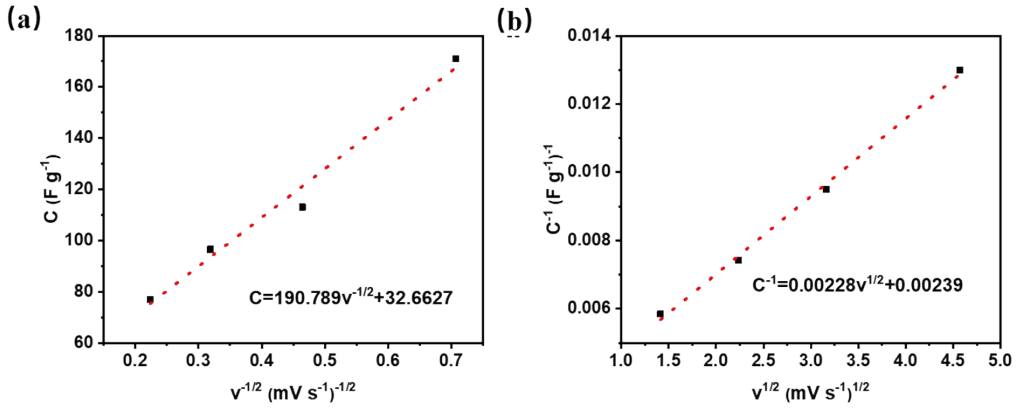

Figure S16. (a) Plots of calculated gravimetric capacity (C) vs. reciprocal of square root of scan rate ($v^{-1/2}$) of the DT-PC. The dash lines are linear fitting lines of data points. The algebraic equations of the fitting lines are shown in corresponding figures. (b) Plots of reciprocal of calculated gravimetric capacity (C^{-1}) vs. square root of scan rate ($v^{1/2}$) of the DT-PC. The dash lines are linear fitting lines of data points. The algebraic equations of the fitting lines are shown in corresponding figures.

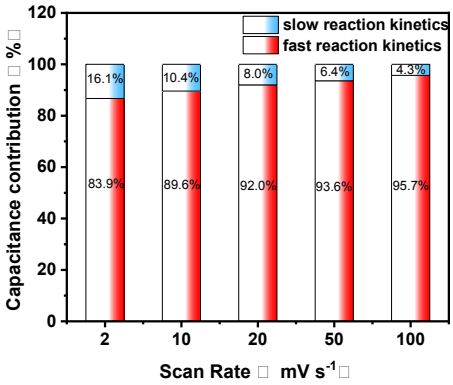

Figure S17. Histograms of the capacitance contributions by the different processes of ST-PC sample.

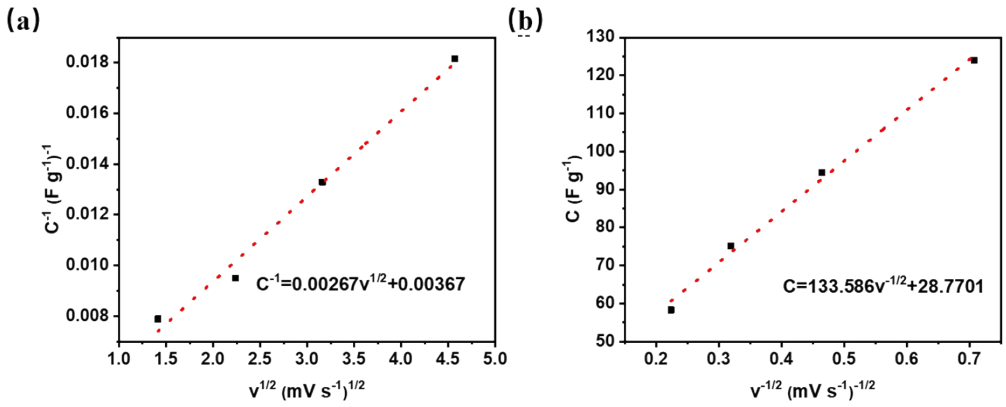

Figure S18. (a) Plots of calculated gravimetric capacity (C) vs. reciprocal of square root of scan rate ($v^{-1/2}$) of the ST-PC. The dash lines are linear fitting lines of data points. The algebraic equations of the fitting lines are shown in corresponding figures. (b) Plots of reciprocal of calculated gravimetric capacity (C^{-1}) vs. square root of scan rate ($v^{1/2}$) of the ST-PC. The dash lines are linear fitting lines of data points. The algebraic equations of the fitting lines are shown in corresponding figures.

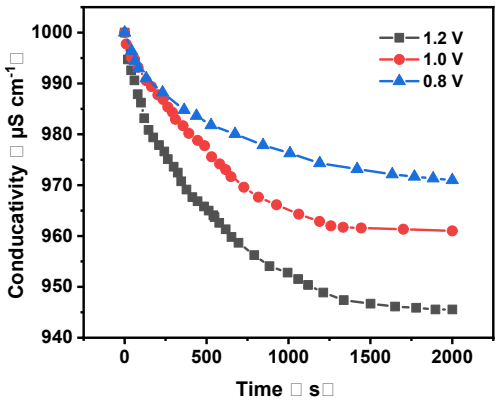

Figure S19. Variation of solution conductivity vs. time at different voltages.

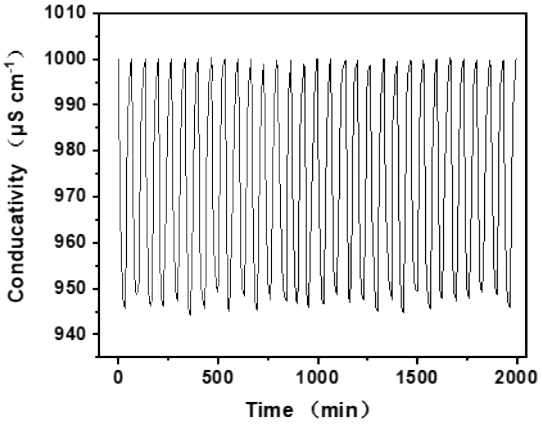

Figure S20. Adsorption-desorption cycle tests of DT-PC.

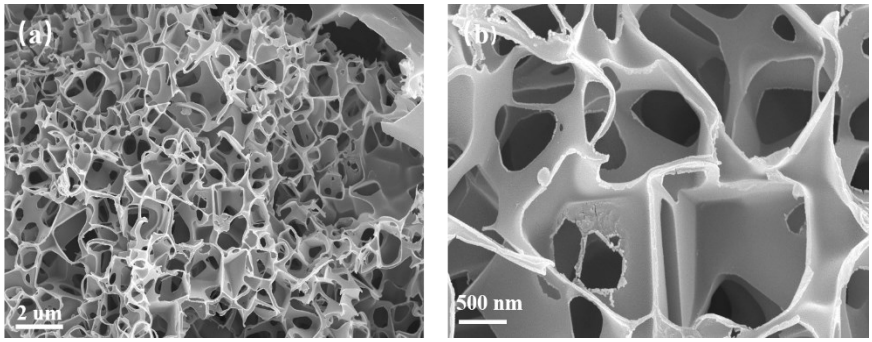

Figure S21. SEM images of DT-PC sample after 30 adsorption-desorption cycles

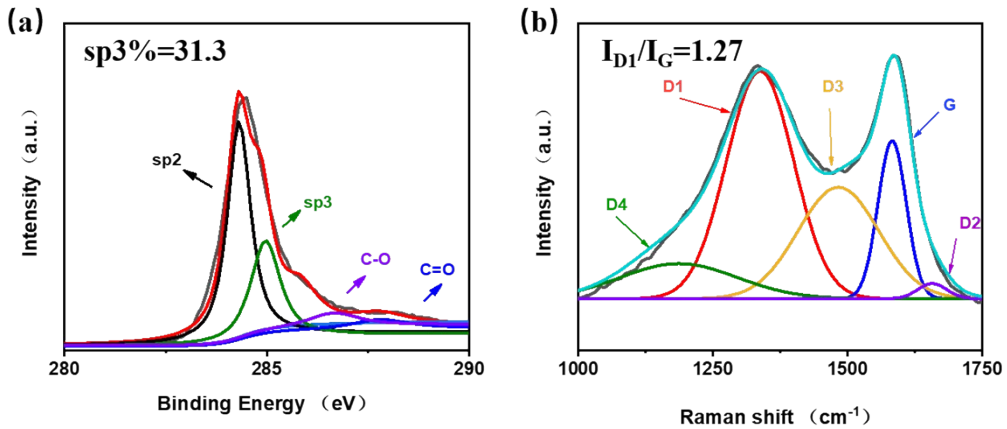

Figure S22. (a) C1s spectrum; (b) Raman spectroscopy of DT-PC after 3030 adsorption-desorption cycles.

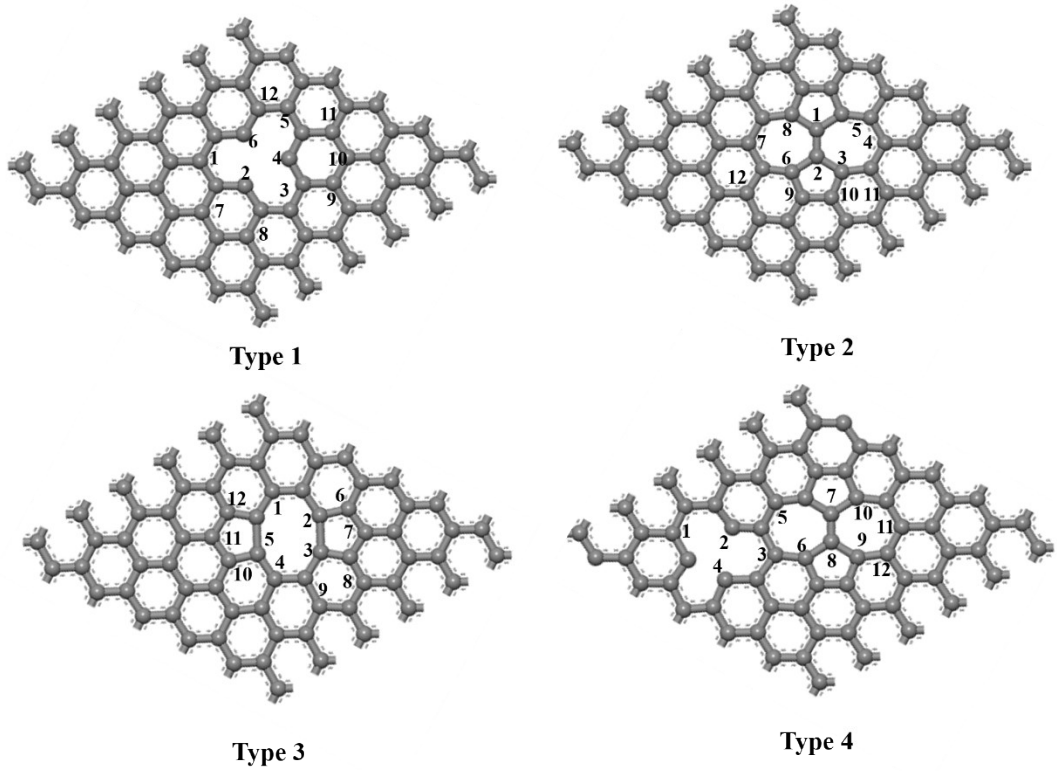

Figure S23. Models of graphene with single vacancy defects, Stone-Wales defects, di-vacancy defects and the combination of single vacancy defects and Stone-Wales defects.

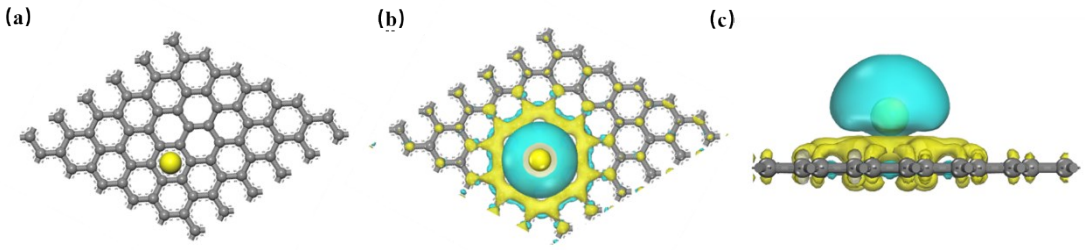

Figure S24. Theoretical simulations and related results. (a) The Na atom is absorbed by the ideal graphite structure. (b, c) Top view and side view of the difference in electron density of Na absorbed in ideal graphite structure.

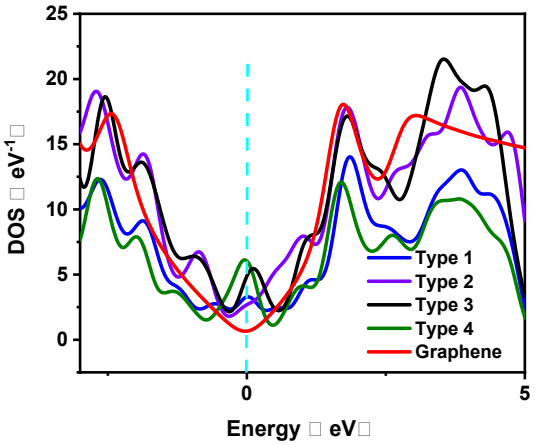

Figure S25. DOS profiles of different carbon defects.

S2. Theoretical Calculations

The spin-polarized density functional theory (DFT) calculations were all performed by using the plane wave basis set based Vienna ab initio simulation package (VASP). Perdew-Burke-Ernzerhof (PBE) functional was adopted to describe the interaction between electrons and the cutoff energy of 400 eV was adopted for plane wave basis set. All the atoms were allowed to relax until the residue forces on each atom were less

than 0.02 eV/Å. The graphene model used in our calculation consists of 12.30 × 29.83 × 15.00 $Å^3$. The vacuum region was set 20 Å in z direction to prevent the interaction between two adjacent surfaces. A 5×1×1 Monkhorst-Pack sampled k-points in the irreducible Brillouin zone for structure optimization. All the configurations are built by Material studio (MS).

To evaluate the stability of Na adsorbed on graphene nanoribbons, we calculated the adsorption energy (E_{ads}) of one Na on the surface as follows,

$$E_{ads} = E_{tot} - E_{surf} - E_{Na}$$

E_{tot} and E_{surf} are the total energies of graphene with and without Na adsorption, E_{Na} is the energy for single Na involved its bulk structures.

Table S1 Chemical compositions of as-prepared samples calculated from XPS results.

Samples	at.% C	at.% O	sp2	sp3	C-O	C=O
DT-PC	94.7	5.3	63.2%	32.2%	4.4%	0.2%
ST-PC	93.4	6.7	70.1%	24.9%	4.8%	0.2%
NT-C	88.6	11.4	79.4%	11.5%	8.9%	0.2%

Table S2 The Raman bands and vibration modes of graphite.

Band	Raman shift (cm^{-1})	Vibration mode
G	~1580	Ideal graphitic lattice
D1	~1350	Disordered graphitic lattice (graphene layer edges)
D2	~1620	Surface graphene layer
D3	~1490	Amorphous carbon
D4	~1200	Polyenes, ionic impurities

Table S3 Physical parameters of the prepared carbon materials.

Samples	I_D/I_G	I_{D1}/I_G	S_{BET} ($m^2\ g^{-1}$)	V_t [a] ($cm^3\ g^{-1}$)	V_{mic} [b] ($cm^3\ g^{-1}$)
DT-PC	1.19	1.28	588	0.39	0.34
ST-PC	1.07	1.16	431	0.27	0.21
NT-C	0.89	0.94	163	0.08	0.07

[a] The total pore volume (V_t); [b] The micropore volume (V_{mic}).

Table S4. Coefficients of Langmuir model fitting.

Isotherm	Model equation	Samples	q_m	K_L	r^2
Langmuir	$q = \frac{q_m K_L C}{1 + K_L C}$	DT-PC	79.2	0.0069	0.999
		ST-PC	56.5	0.0035	0.997
		AC	41.7	0.0029	0.992

Table S5. comparison of salt adsorption capacity with DT-PC and previous literatures.

Sample	Voltage (V)	Initial Concentration (mg/L)	Salt adsorption capacity (mg/g)	Ref.
GO-Mw-Hyd	1.4	500	21.58	1
NPC	1.2	500	21.4	2
DCN	1.2	500	20.9	3
N and P-doped 3D graphene	1.6	800	20.7	4
porous carbon derived from MOGs	1.4	500	25.16	5
activated carbon with functionalized graphene	1.6	30	15.17	6
hierarchical mesoporous carbon derived from ZIF-8	1.2	500	13.89	7
Hierarchical porous carbon derived from activated biochar	1.2	116	8.11	8

ultrathin nitrogen-doped carbon/graphene	1.2	500	17.52	9
boron carbon nitride nanosheets	1.4	500	13.6	10
hole-enhanced 3D graphene	2	572	29.6	11
Carbon Nanocage	1.4	250	17.5	12
N-doped carbon sphere and holey graphene hydrogel	1.4	500	17.8	13
graphene nanosphere decorated N-doped layered mesoporous carbon	1.2	500	23.4	14
highly-ordered mesoporous carbon	1.2	500	14.6	15
Nitrogen-rich mesoporous carbons	1.2	1000	31.3	16
N-doped rod-like porous carbon	1.2	500	24.2	17
B/N doped carbon nanosheets decorated with MnO_2	1.2	500	20.3	18
hierarchically porous non-carbon	1.2	500	23.6	19
N/P-porous carbon	1.4	250	18.1	20
DT-PC	1.2	500	32.4	This work

1 W. Dianbudiyanto, S. Liu, Desalination, 2019, 468, 114069.

2 H. Wang, T. Yuan, L. Huang, W. Yang, Sci. Total Environ., 2020, 720, 137637.

3 Y. Liu, X. Zhang, X. Gu, N. Wu, R. Zhang, F. Huo, Micropor. Mesopor. Mater., 2020, 303, 110303.

4 D. Han, C. Zhang, J. Guan, L. Gai, R. Yue, L. Liu, X. Sun, Electrochim. Acta, 2020, 135639.

5 Z. Wang, T. Yan, G. Chen, L. Shi, D. Zhang, ACS Sustainable Chem. Eng., 2017, 5, 11637-11644.

6 S. Hu, K. Xie, X. Zhang, S. Zhang, J. Gao, D. Chen, Chem. Eng. J., 2020, 384, 123317.

7 T. Gao, Z. Liu, H. Li, Sep. Purif. Technol., 2020, 231, 115918.

8 D. Cuong, P. Wu, N. Liu, C. Hou, Sep. Purif. Technol., 2020, 242, 116813.

9 M. Wang, X. Xu, J. Tang, L. Pan, Y. Yamauchi, Chem. Commun., 2017, 53, 10784.

10 S. Wang, G. Wang, T. Wu, Y. Zhang, F. Zhan, Y. Wang, J. Qiu, J. Mater. Chem. A, 2018,6, 14644-14650.
11 J. Li, B. Ji, R. Jiang, P. Zhang, N. Chen, L. Qu, Carbon, 2018, 129, 95-103.
12 X. Zang, Y. Xue, W. Ni, C. Li, L.n Hu, A. Zhang, Y. Yan, ACS Appl. Mater. Interfaces 2020, 12, 2, 2180-2190.
13 M. Mi, X. Liu, W. Kong, Y. Ge, W. Dang, J. Hu, Desalination, 2019, 464, 18-24.
14 O. Noonan, Y. Liu, X. Huang, C. Yu, J. Mater. Chem. A, 2018, 6, 14272.
15 X. Xu, H. Tan, L. Pan, T. Yang, Y, Yamauch, Environ. Sci.: Nano, 2019, 6, 981.
16 Y. Zhao, Y. Zhang, K. Li, C. Lv, Electrochim. Acta, 2019, 321, 134665.
17 J. Zhang, T. Yan, J. Fang, L. Shi, D. Zhang, Environ. Sci.: Nano, 2020,7, 926-937.
18 Z. Xie, X. Shang, J. Yang, B. Hu, J. Liu, Carbon, 2020, 158, 184-192.
19 Y. Wu, G. Jiang, A. Yu, Z. Zhang, Z. Chen, J. Mater. Chem. A, 2019, 7, 15633.
20 S. Huo, Y. Zhao, M. Zong, K. Li, J. Mater. Chem. A, 2020, 8, 2505.

Table S6. Bader charge analysis.

	Charge state (e)				
Atom	Type 1	Type 2	Type 3	Type 4	Pristine graphene
1	-0.1030	-0.0438	-0.1706	-0.1445	0.0036
2	-0.0289	-0.1109	-0.0125	0.0679	0.0036
3	-0.0067	0.0788	0.0119	-0.0144	-0.0037
4	0.0797	0.0104	-0.0368	0.1174	-0.0035
5	-0.0566	0.2077	0.0559	-0.0308	0.0039
6	0.0498	0.0910	0.1215	-0.0168	0.0036
7	-0.0481	-0.2679	0.0172	-0.0174	0.0037
8	0.0705	0.1160	0.2291	0.0796	-0.0035
9	0.1117	0.0634	0.0847	-0.1076	-0.0037
10	0.1484	0.0410	0.0426	0.1582	0.0036
11	0.0249	0.0228	-0.0411	-0.1123	-0.0038
12	0.0566	0.0093	-0.1423	-0.0895	0.0037